Supplementary Materials for

On the Attraction of Marine Dunes to OWF Fixed Foundations

Noémie Durand, Pablo Tassi, Olivier Blanpain, Alice Lefebvre

*Corresponding author: noedurand@openbook.team
Paper DOI: 10.59236/geomorphica.v2i1.44

Table of Contents:

Supplementary Text

The openTELEMAC system is a state-of-the-art free surface flow suite of solvers based on the finite element method, on unstructured grids. It comprises several modules, each describing different physical processes, of which TELEMAC-3D is the three-dimensional hydrodynamic module (Hervouet, 2007), and GAIA the sediment transport and bed evolution module (Tassi et al., 2023).

TELEMAC-3D solves the 3D Navier-Stokes equations. We use the so-called 'non-hydrostatic' form, with no assumption on the pressure. Together with the continuity equation (A1), the Navier-Stokes equations are written in Cartesian coordinates as:

$$\vec{\nabla} \cdot \vec{U} = S_h \tag{A1}$$

$$\partial_t \vec{U} + (\vec{U} \cdot \vec{\nabla}) \vec{U} = -\frac{1}{\rho} \vec{\nabla} p + \upsilon \Delta \vec{U} + \vec{g} + \vec{S} \tag{A2}$$

where t denotes the time (s). ρ is the density of the fluid (kg m^{-3}); υ the kinematic viscosity (m^2 s^{-1}); and $\vec{g}$ the gravitational acceleration (m s^{-2}). The S terms are source and sink terms in the different equations: S_h (s^{-1}) represents a flux of water such as rain, evaporation or discharges ($S_h = 0$ for this work); $\vec{S}$ (m s^{-2}) represents contributions from the wind, waves or bottom friction for example. The pressure p (Pa) and the three velocity components $\vec{U} = (u,v,w)$ (m s^{-1}) are the unknowns, computed at each node and layer of the computational domain.

Wind forcing appears in Equation A2 through the two-dimensional condition at the surface:

$$\upsilon\, \partial_n \vec{U}_H = \frac{\vec{\tau}_{wind}}{\rho} = \frac{\rho_{air}}{\rho}\, a_{wind}\, ||\vec{V}_{10m}||\vec{V}_{10m} \tag{A3}$$

where $\vec{U}_H$ denotes the horizontal velocity at the surface and $\vec{\tau}_{\mathrm{wind}}$ the wind stress, expressed in Heaps (1965) and Flather (1979) in terms of a quadratic function of the wind velocity, $\vec{V}_{\mathrm{10m}}$, commonly defined 10 m above sea level. a_{wind} is a dimensionless drag coefficient, dependent on the wind velocity, and hiding complex phenomena (e.g., sea surface roughness, wind speed, fetch). In Equation A3, ρ_{air} is the air density (kg m^{-3}).

Atmospheric pressure gradients are integrated with the source terms:

$$\vec{S}_{atm} = -\frac{1}{\rho} \vec{\nabla}\, p_{atm} \tag{A4}$$

where p_{atm} denotes the atmospheric pressure at sea level.

TELEMAC-3D is internally coupled with GAIA to provide the conditions that drive the sediment transport and bed evolution processes. The coupling strategy adopted in the openTELEMAC system is based on synchronous-decoupled techniques. TELEMAC-3D computes the hydrodynamic solution for a given (fixed) bathymetry. GAIA is then called to update the seabed levels according to the revised hydrodynamics. The revised bathymetry is fed back into TELEMAC-3D. This loop is repeated at each model time step.

The change in bed level is computed in GAIA by solving the sediment mass conservation equation, also known as the Exner equation. This equation expresses the fact that bed levels rise in proportion to the amount of sediment that is no longer transported, and conversely, lower in proportion to the amount of sediment that is entrained by the flow. In its simplest form (bedload transport of one class of non-cohesive sediment), this equation reads:

$$(1-\lambda_p)\,\partial_t\left(\rho_s z_b\right)+\vec{\nabla}\cdot\vec{Q}_{mb}=0 \tag{A5}$$

where z_b denotes the bottom elevation (m) and λ_p the bed porosity. $\vec{Q}_{\mathrm{mb}} = (Q_{mb,x}, Q_{mb,y})$ is the bedload mass transport rate $= \rho_s\,\vec{Q}_{\mathrm{b}}$ (kg m^{-1} s^{-1}), with ρ_s the sediment density (kg m^{-3}).

Total sediment transport can be divided into suspended sediment transport, where sediment put in suspension by the turbulence of the flowing water is transported by the ambient current, and bedload transport, where sediment is transported in almost continuous contact with the bed, by rolling, sliding or being carried by saltation. Suspended sediment transport is not explicitly considered in this work and will not be expanded upon here. Bedload transport is taken into account by computing bedload fluxes in accordance with formulations published in the literature.

We have used the formulation proposed by Soulsby and van Rijn (Soulsby, 1997), which reads in the absence of wave processes:

$$\vec{Q}_b=(A_{sb}+A_{ss})\,\vec{U}_{2D}\left[\,\|\vec{U}_{2D}\|-U_{cr}\right]^{2.4} \tag{A6}$$

where $\vec{Q}_{\mathrm{b}}$ is the volumetric transport rate per unit width (m^2 s^{-1}). $A_{sb} = f\,(h^{-0.2})$ denotes the bedload coefficient (h the water depth), $A_{ss} = f\,(d_{50}{}^{-0.8})$ the suspended load coefficient. These coefficients had originally been derived for rivers, both from physical and empirical considerations. They are valid for water depths between 1 and 20 m, depth-averaged velocities of between 0.5 and 5 m s^{-1} and sediment grains between 0.1 and 2 mm. $\vec{U}_{2\mathrm{D}}$ is the depth-averaged current velocity and $\|\vec{U}_{2D}\|$ its norm; $U_{cr} = f\,(d_{50},\ h\,/\,d_{90})$ the threshold velocity defined by van Rijn (1984).

The performance of sediment transport predictors is known to vary considerably (Camenen and Larroudé, 2003; van Rijn et al., 2001) and it is generally accepted that estimates of sediment transport rates are valid within a factor of 2 to 5, particularly in coastal environments. The modern consensus is that the Soulsby and van Rijn predictor (Equation A6) tends to overestimate the sediment transport rate. A scaling factor was introduced in this application. It is critical to note that this scaling factor is a calibration parameter specific to the conditions of this study and not a general correction to the underlying formulation.

Supplementary Figures

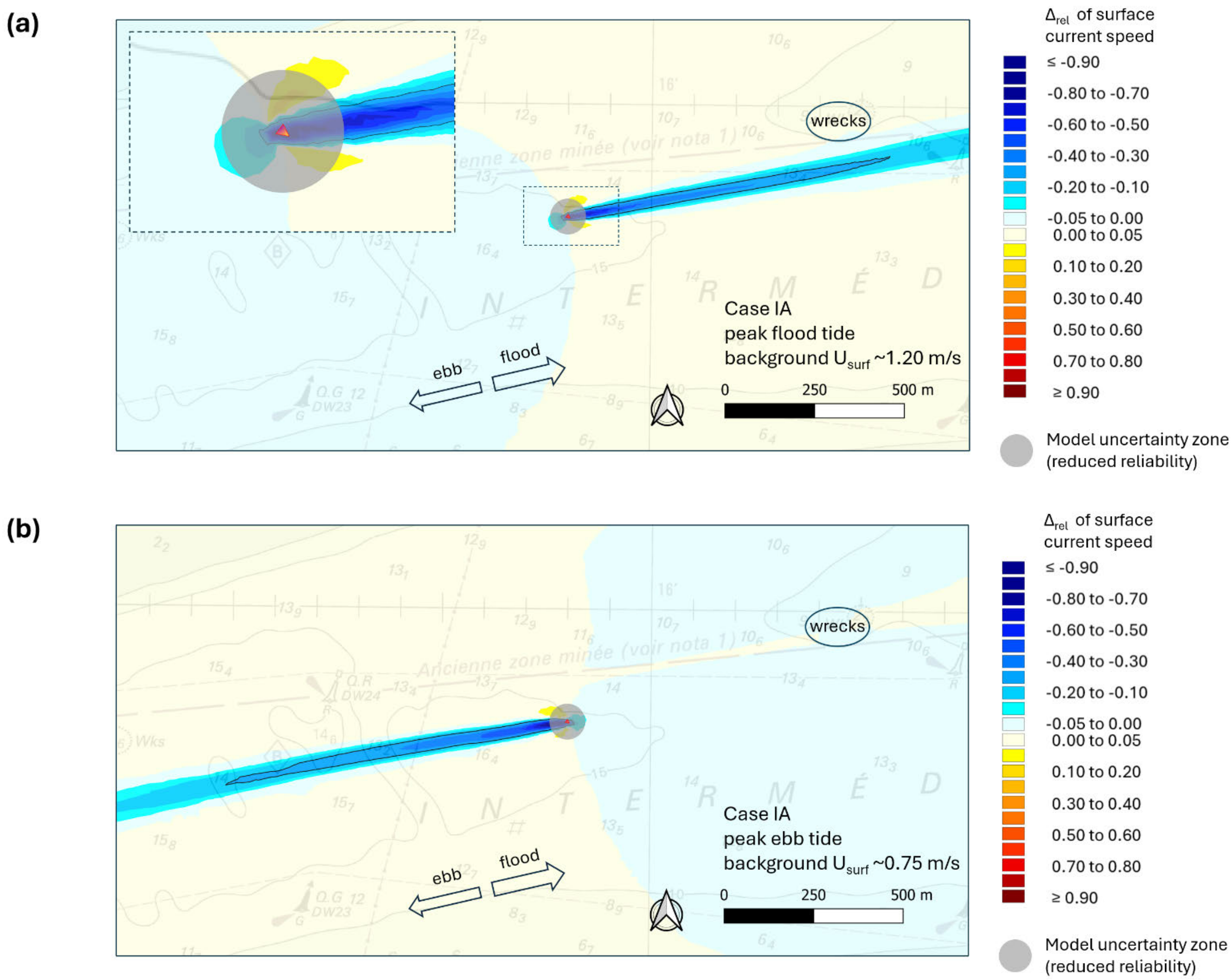

Figure S1

Relative difference in surface velocity (Δrel, as defined in Rivier et al., 2016, using their colour scheme for direct comparison) for Case IA during (a) a representative flood tide and (b) a representative ebb tide. The black contour line denotes Δrel = -0.20. The inset in (a) shows a detailed view of the region marked by the dashed box, highlighting the orientation of the monopile (filled triangle to scale) to the flow. The greyed-out zone in all panels denotes an area of potential model uncertainty within a 50 m radius of the monopile, where local processes are not explicitly simulated (Background data source: Shom nautical chart 7057).

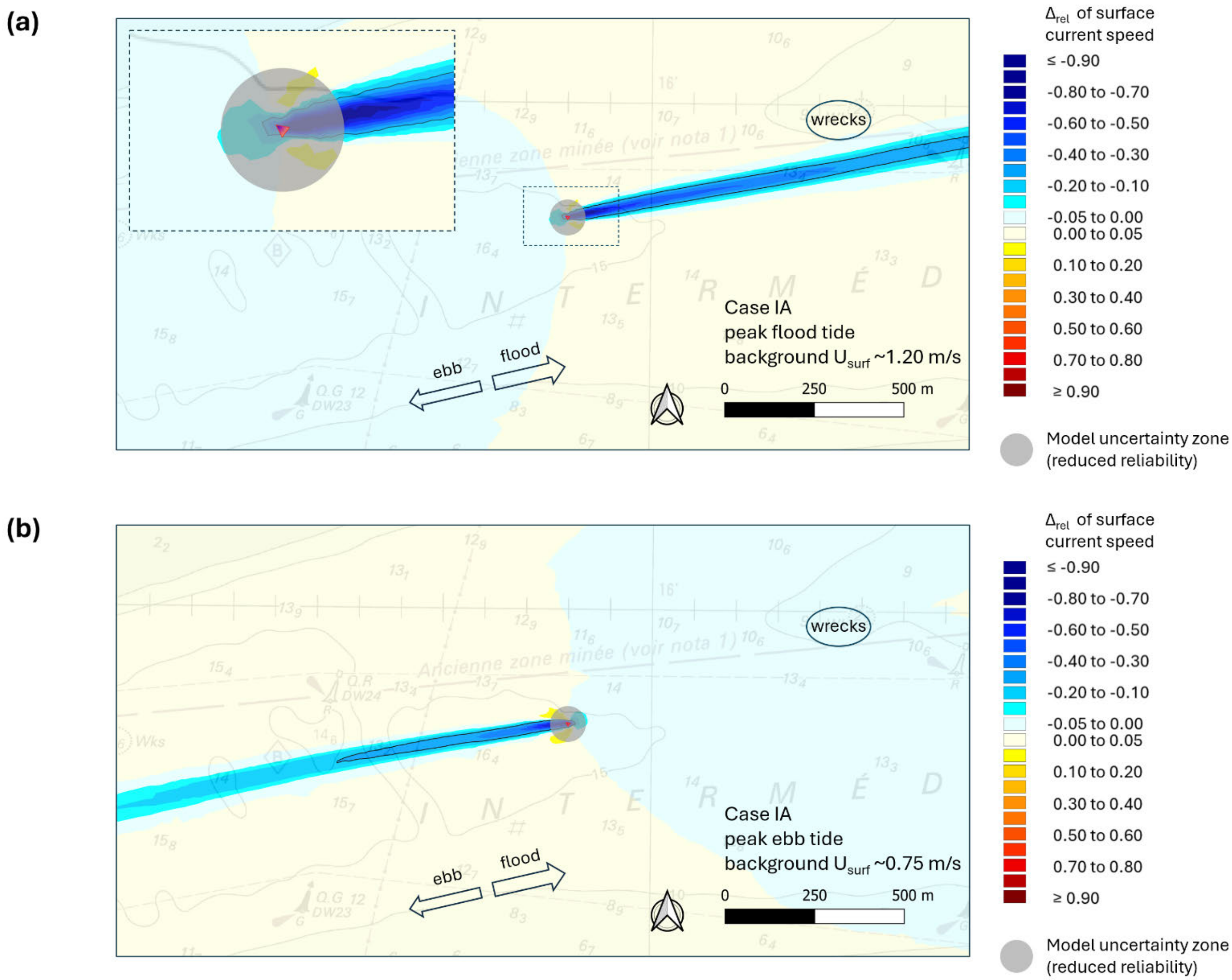

Figure S2

Relative difference in surface velocity (Δrel) during (a) the same representative flood tide and (b) the same representative ebb tide as in Figure S1. The black contour line denotes Δrel = -0.20. The inset in (a) shows a detailed view of the region marked by the dashed box, highlighting the different orientation of the monopile (filled triangle to scale) compared to Case IA. The greyed-out zone in all panels denotes an area of potential model uncertainty within a 50 m radius of the monopile, where local processes are not explicitly simulated (Background data source: Shom nautical chart 7057).

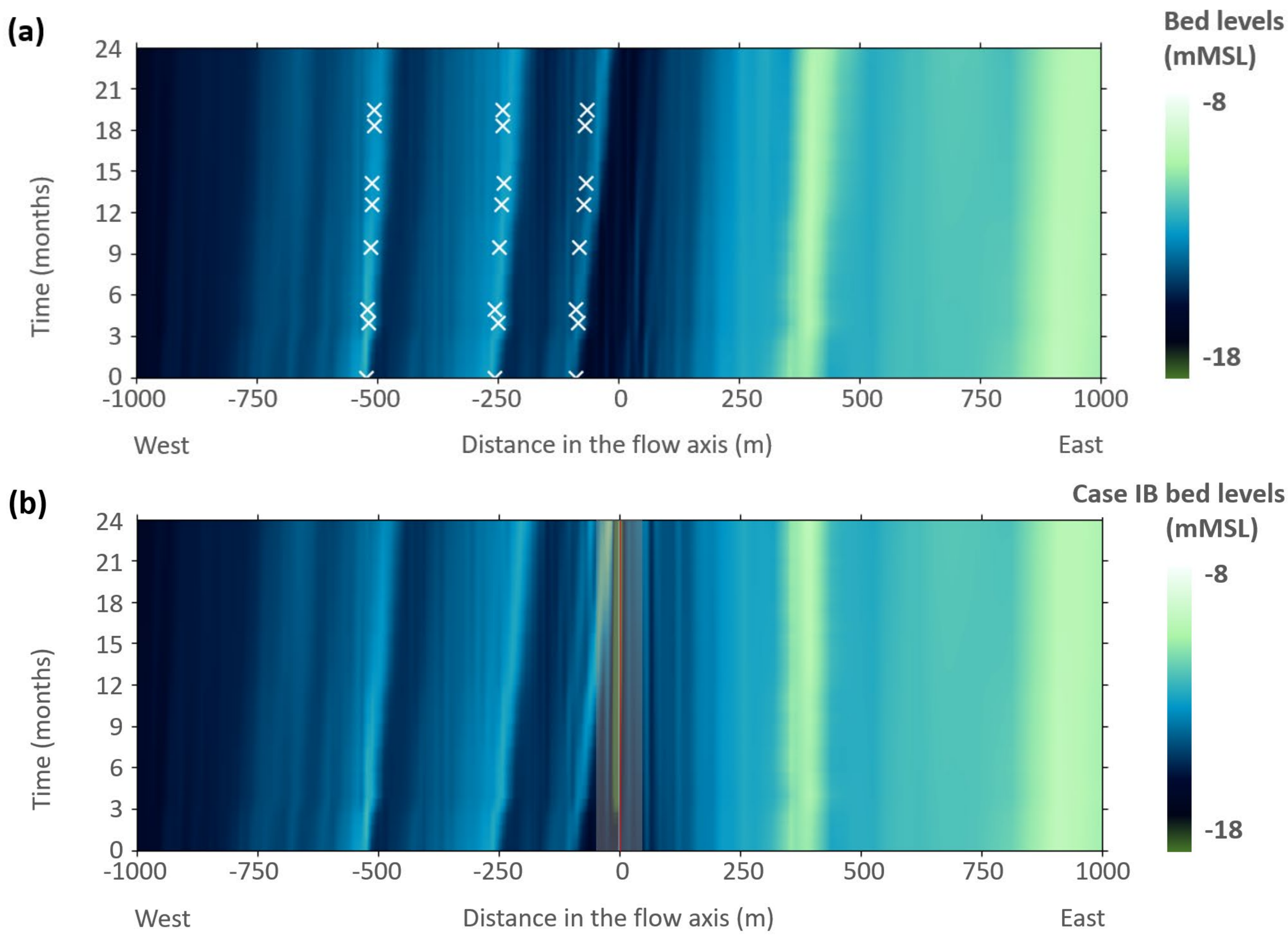

Figure S3

Temporal evolution of bed levels extracted along the tidal axis through the monopile (a) from the baseline simulation and (b) from the Case IB simulation, where the monopile is marked by the red line. White crosses in panel (a) mark available measured data from the bathymetric surveys conducted between November 2019 and July 2021 (FEM, 2021). The greyed-out zone in panel (b) denotes an area of potential model uncertainty within a 50 m radius of the monopile, where local processes are not explicitly simulated.

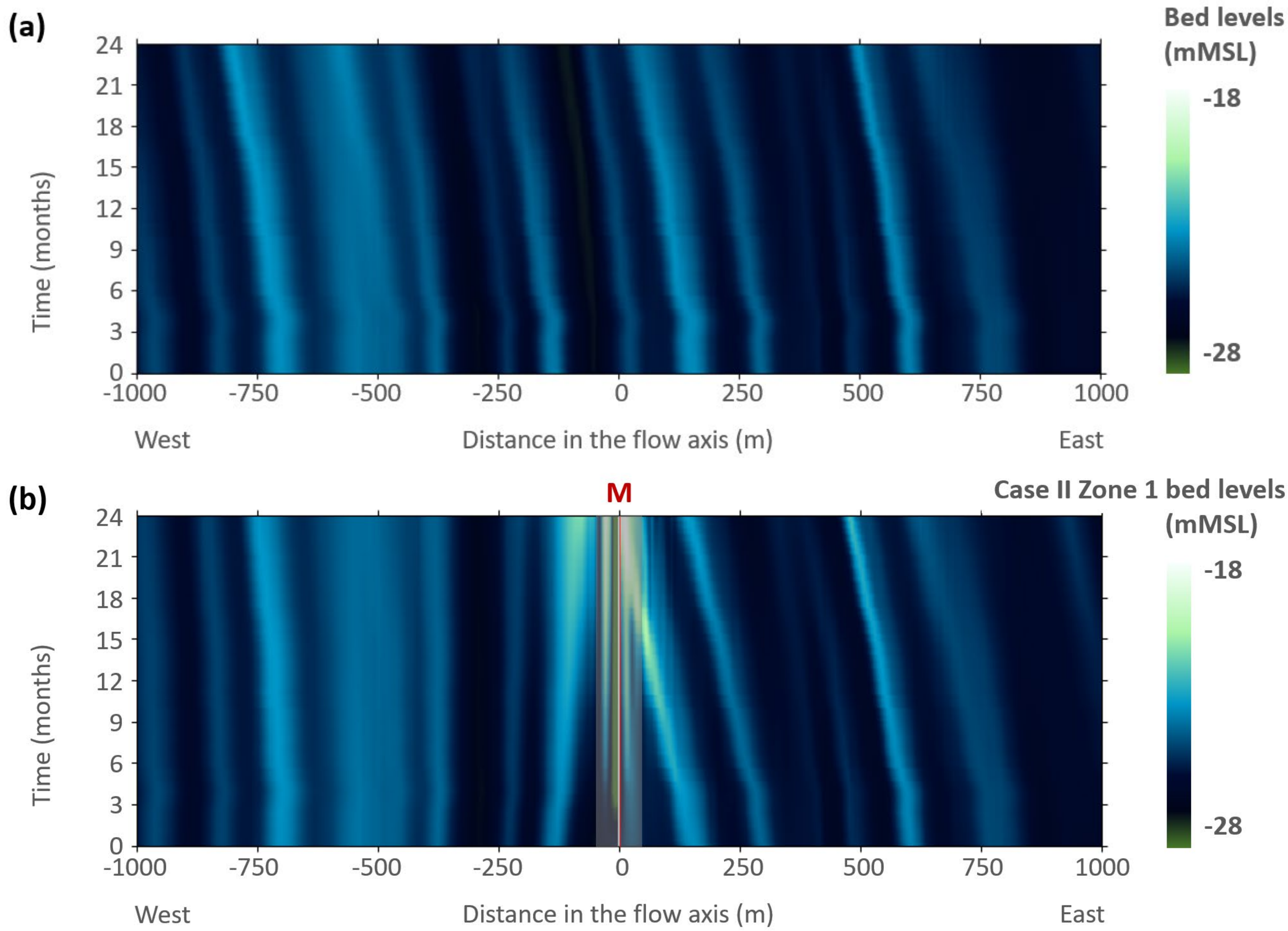

Figure S4

Temporal evolution of bed levels extracted in Zone 1: (a) for the baseline simulation and (b) for the Case II simulation, along the tidal axis through the monopile marked 'M' in Figure 7 (b) and identified by the red line. The greyed-out zone in panel (b) denotes an area of potential model uncertainty within a 50 m radius of the monopile, where local processes are not explicitly simulated.

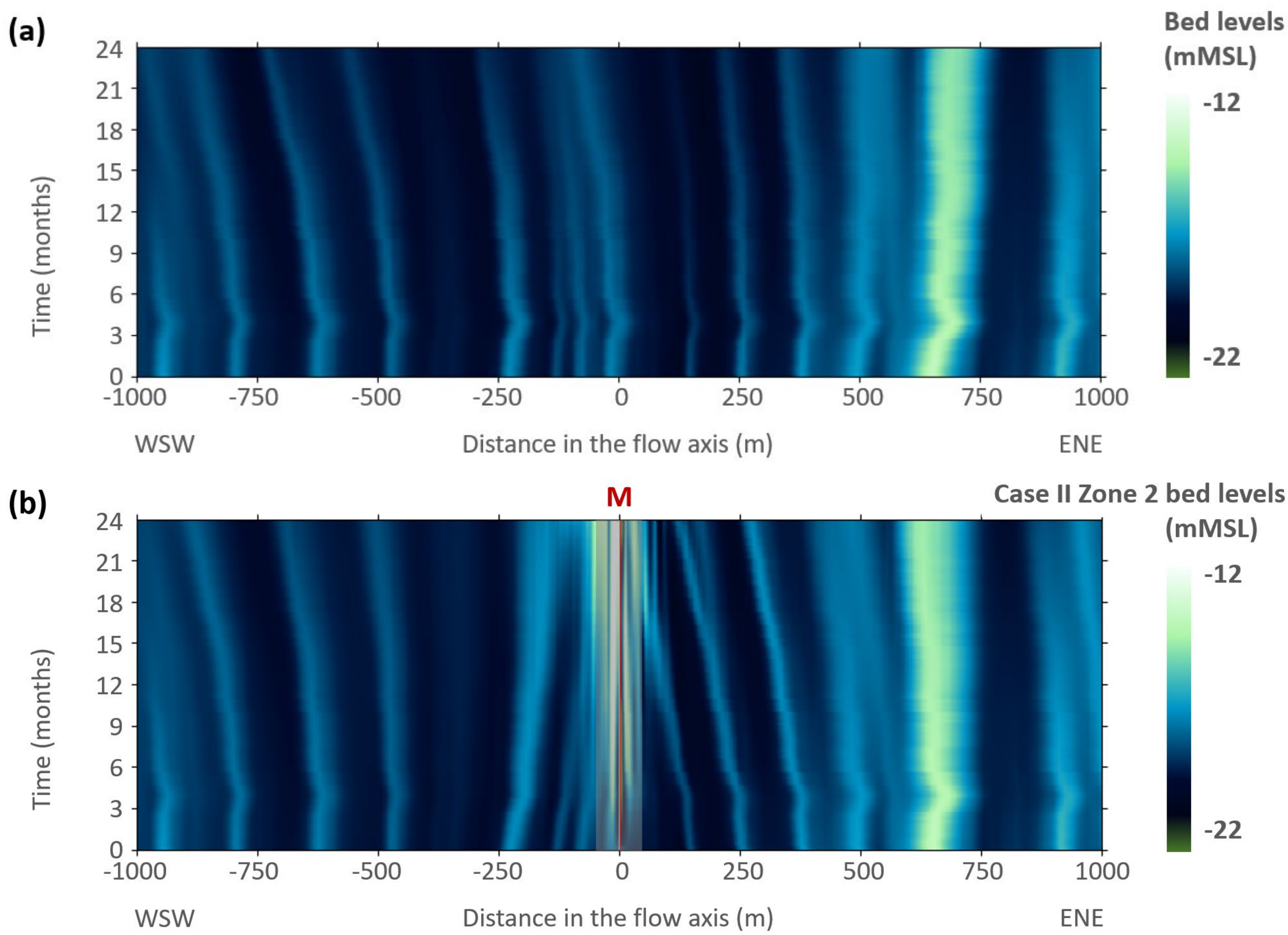

Figure S5

Temporal evolution of bed levels extracted in Zone 2: (a) for the baseline simulation and (b) for the Case II simulation, along the tidal axis through the monopile marked 'M' in Figure 7 (c) and identified by the red line. The greyed-out zone in panel (b) denotes an area of potential model uncertainty within a 50 m radius of the monopile, where local processes are not explicitly simulated.

Supplementary Tables

Table S1

Predicted displacement of marine dune crests after one year along the transverse profiles used for Case IA in Figure 6 and for Case IB in Figure S1. The transects are oriented from west to east, with 0 marking the monopile location. Positive displacement values indicate eastward propagation. For reference, the seabed profiles taken directly from the model are also displayed.

Initial crest location along transect	Displacement in the baseline scenario (natural state)	Displacement in a scenario with a monopile	Acceleration rate
		Case IA	
-801.7 m	59.1 m	92.1 m	56%
-262.7 m	41.3 m	75.9 m	84%
-104.5 m	45.9 m	82.0 m	79%
142.0 m	41.3 m	-30.0 m	-173%
312.2 m	40.2 m	-22.4 m	-156%

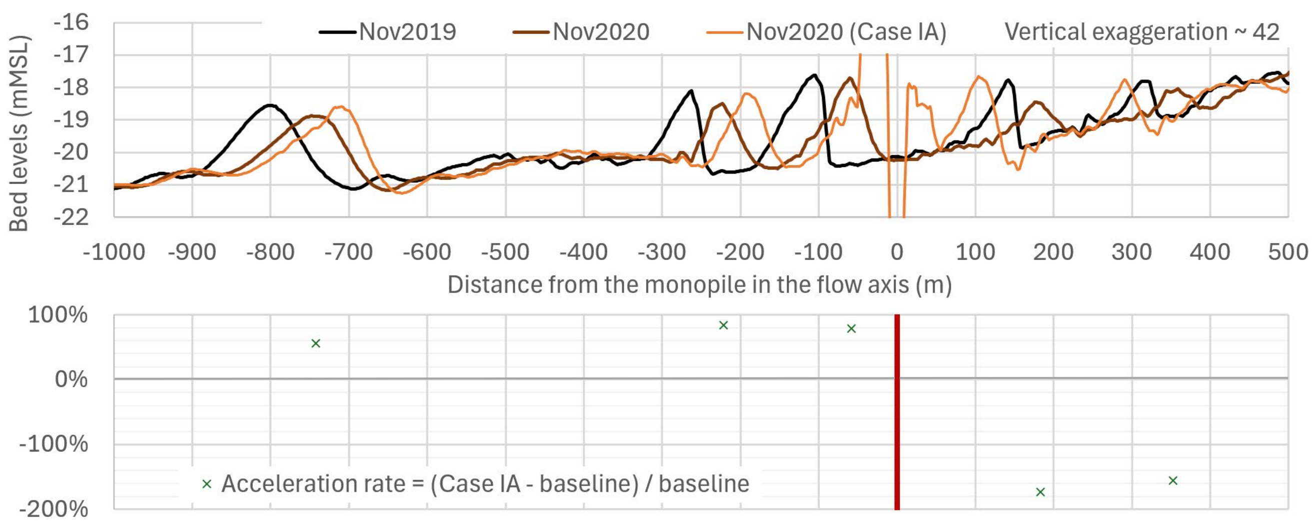

Initial crest location along transect	Displacement in the baseline scenario (natural state)	Displacement in a scenario with a monopile Case IB	Acceleration rate
-523.5 m	27.5 m	31.5 m	15%
-261.3 m	28.9 m	35.8 m	24%
-104.1 m	41.8 m	47.4 m	13%
388.0 m	19.8 m	5.4 m	-73%

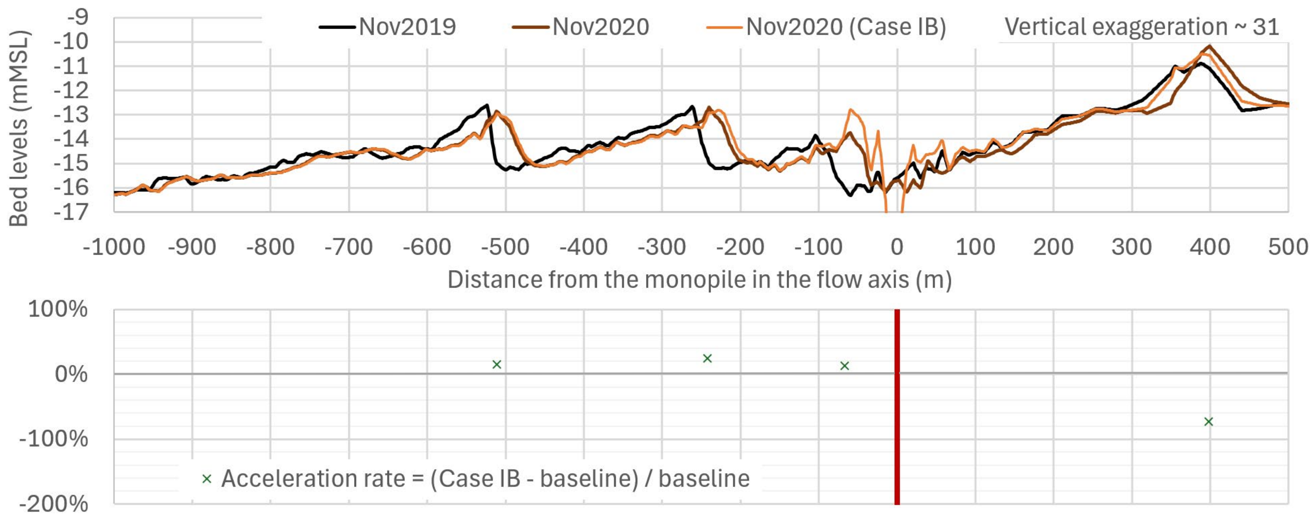

Table S2

Predicted displacement of the marine dune crests after one year along transverse profiles through the monopiles marked 'M' in Figure 7. The transects are oriented from west to east, with 0 marking the monopile location. Positive displacement values indicate eastward propagation. For reference, the seabed profiles taken directly from the model are also displayed.

Initial crest location along transect	Displacement in the baseline scenario (natural state)	Displacement in Case II with an array of monopiles	Acceleration rate
		Zone 1	
-938.8 m	-38.7 m	-4.1 m	-89%
-802.3 m	-34.7 m	-8.2 m	-76%
-679.9 m	-34.7 m	-6.1 m	-82%
-514.8 m	-18.3 m	-8.2 m	-55%
-353.8 m	-30.6 m	0.0 m	-100%
-209.0 m	-24.5 m	12.2 m	-150%
-113.2 m	-42.8 m	30.6 m	-171%
176.3 m	-48.9 m	-77.5 m	58%
321.0 m	-44.8 m	-71.4 m	59%
506.5 m	-24.5 m	-34.7 m	42%
628.9 m	-48.9 m	-59.1 m	21%
814.4 m	-67.3 m	-83.6 m	24%

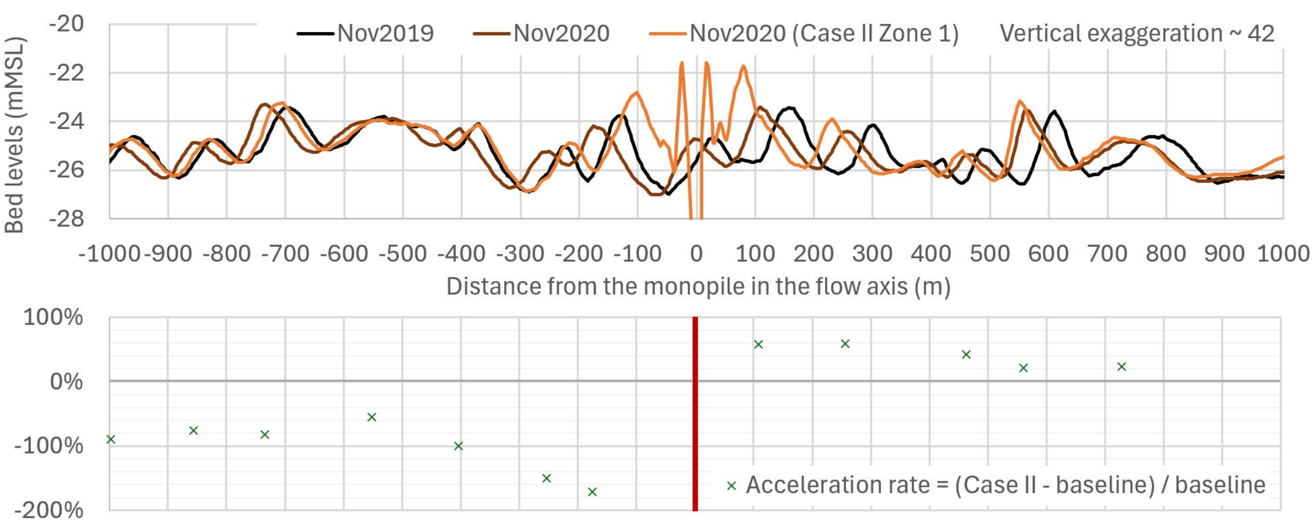

Initial crest location along transect	Displacement in the baseline scenario (natural state)	Displacement in Case II with an array of monopiles	Acceleration rate
		Zone 2	
-773.7 m	-24.5 m	-24.5 m	0%
-604.5 m	-26.5 m	-18.3 m	-31%
-455.7 m	-22.4 m	-2.0 m	-91%
-209.0 m	-2.0 m	42.8 m	-2240%
-111.2 m	--	55.0 m	--
-58.2 m	-18.3 m	--	--
164.1 m	-2.0 m	-63.2 m	3062%
276.2 m	-8.2 m	-57.1 m	596%
396.5 m	0.0 m	-42.8 m	--
512.7 m	16.3 m	-12.2 m	-175%
671.7 m	30.6 m	0.0 m	-100%
934.7 m	20.4 m	-6.1 m	-130%

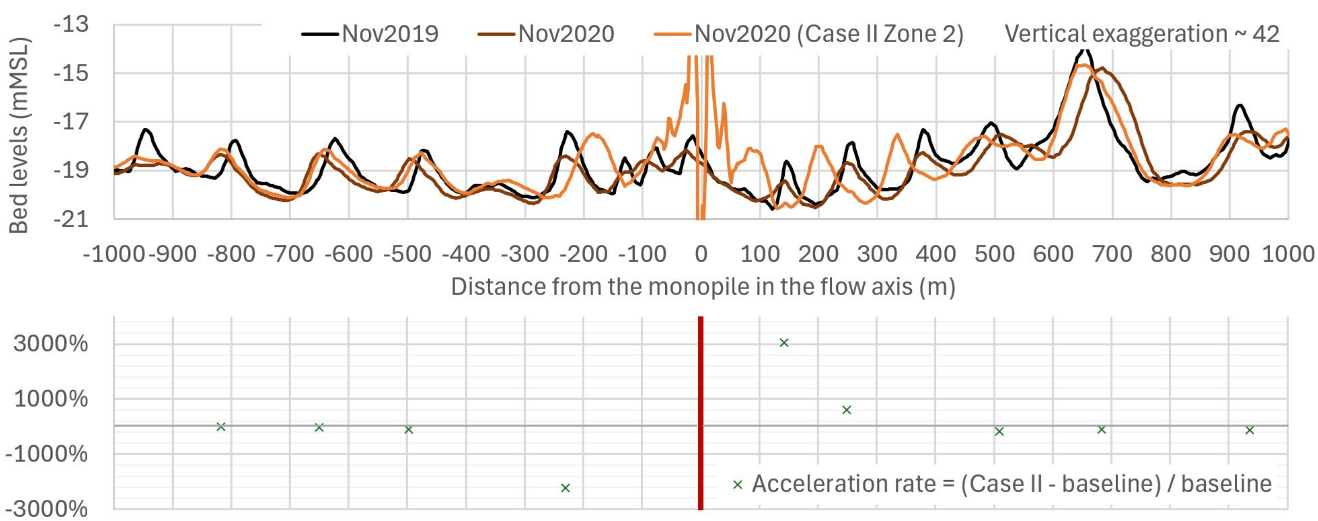

References

Hervouet, J.-M. (2007). Hydrodynamics of free surface flows : Modelling with the finite element method. John Wiley & Sons, Inc. doi: https://doi.org/10.1002/9780470319628

Tassi, P., Benson, T., Delinares, M., Fontaine, J., Huybrechts, N., Kopmann, R., . . . Walther, R. (2023). GAIA - a unified framework for sediment transport and bed evolution in rivers, coastal seas and transitional waters in the TELEMAC-MASCARET modelling system. *Environmental Modelling & Software*, 159, 105544. doi: https://doi.org/10.1016/j.envsoft.2022.105544

Heaps, N. S. (1965). Storm surges on a continental shelf. *Philosophical Transactions of the Royal Society of London. Series A, Mathematical and Physical Sciences*, 257 (1082), 351-383. doi: https://doi.org/10.1098/rsta.1965.0009

Flather, R. A. (1979). Recent results from a storm surge prediction scheme for the North Sea. In *Marine forecasting* (Vol. 25, p. 385-409). Elsevier. doi: https://doi.org/10.1016/S0422-9894(08)71140-1

Soulsby, R. L. (1997). Dynamics of marine sands. Thomas Telford Publishing. doi: https://doi.org/10.1680/doms.25844

van Rijn, L. C. (1984). Sediment transport, part III: Bed forms and alluvial roughness. *Journal of Hydraulic Engineering*, 110 (12), 1733-1754. doi: https://doi.org/10.1061/(ASCE)0733-9429(1984)110:12(1733)

Camenen, B. and Larroudé, P. (2003). Comparison of sediment transport formulae for the coastal environment. *Coastal Engineering*, 48(2):111–132. doi: https://doi.org/10.1016/S0378-3839(03)00002-4

van Rijn, L. C., Davies, A. G., van de Graaff, J., & Ribberink, J. S. (Eds.). (2001). SEDMOC Sediment transport modelling in marine coastal environments. Aqua Publications.

Rivier, A., Bennis, A.-C., Pinon, G., Magar, V., and Gross, M. (2016). Parameterization of wind turbine impacts on hydrodynamics and sediment transport. *Ocean Dynamics*, 66(10):1285–1299. doi: https://doi.org/10.1007/s10236-016-0983-6

FEM. 2019-2021 multi-beam bathymetric surveys conducted as part of pre-feasibility studies for the Dunkirk offshore wind farm area (DUNES project). Proprietary data not available to the public at this time, 2021